



HAL
open science

Aggregation behavior of one-patch inverse patchy particles: an experimental and numerical study

Khaoula Lebdioua, Manuella Cerbelaud, Anne Aimable, Arnaud Videcoq

► **To cite this version:**

Khaoula Lebdioua, Manuella Cerbelaud, Anne Aimable, Arnaud Videcoq. Aggregation behavior of one-patch inverse patchy particles: an experimental and numerical study. 2020. hal-02613670

HAL Id: hal-02613670

<https://hal.science/hal-02613670>

Preprint submitted on 20 May 2020

HAL is a multi-disciplinary open access archive for the deposit and dissemination of scientific research documents, whether they are published or not. The documents may come from teaching and research institutions in France or abroad, or from public or private research centers.

L'archive ouverte pluridisciplinaire **HAL**, est destinée au dépôt et à la diffusion de documents scientifiques de niveau recherche, publiés ou non, émanant des établissements d'enseignement et de recherche français ou étrangers, des laboratoires publics ou privés.

Aggregation behavior of one-patch inverse patchy particles: an experimental and numerical study

Khaoula Lebdioua, Manuella Cerbelaud*, Anne Aimable*, Arnaud Videcoq
Univ. Limoges, CNRS, IRCER, UMR 7315, F-87000 Limoges, France

Abstract

Hypothesis

Inverse patchy colloids (IPCs) are promising building blocks to create new materials using their self-organization. For example, the control of the self-assembly of oxide-based IPCs is interesting for ceramic shaping. Thus, the synthesis of silica based IPCs as well as a detailed study of their behavior in suspension are presented in this paper.

Experiments

Fluorescent silica particles are partially modified in surface by grafting amine groups using a Pickering emulsion route. Zeta potential measurements, sedimentation tests and confocal microscopy observations are carried out to analyze the aggregation of the obtained particles in aqueous suspension as a function of the patch size and of the pH. Brownian dynamics simulations are also performed to better understand the aggregate structures.

Findings

The aggregation of the synthesized silica-based IPCs can be tuned by modifying both the patch size and the pH of the suspensions. Different aggregate structures, from elongated to compact ones, are obtained. This control of aggregation makes such particles promising to build new ceramic materials.

Keywords: Colloid; Aggregation; Inverse patchy particles; Brownian dynamics simulations; Confocal microscopy

*Corresponding author

Email addresses: manuella.cerbelaud@unilim.fr; Tel: +33 (0)5 87 50 23 47 (Manuella Cerbelaud), anne.aimable@unilim.fr; Tel: +33 (0)5 87 50 23 68 (Anne Aimable)

1. Introduction

Colloid science is crossing multiple scientific disciplines, such as food and nutrition, cosmetics, biology, soft matter, nanophysics, or nanomaterials [1]. Colloidal interactions depend on the surface chemistry and the chemical environment of the colloids, which both determine their surface charge, and their hydrophilic or hydrophobic properties. Researchers have addressed this field from a long time with both experimental and fundamental studies, as many real problems may be solved through a better understanding and control of colloidal interactions; for example aggregation in biological fluids, or clogging in industrial processes. To describe real systems with more accuracy (for example proteins often carry different surface charges), anisotropic particles with inhomogeneous surface properties have been studied. Various morphologies exist: Janus particles, which present two different hemispheres, or patchy particles, with one or several different chemical functions or materials present on a smaller fraction of the surface. These anisotropic particles are able to assemble in more complex structures to achieve original clusters, mimicking molecular or crystal arrangements at the colloidal scale [2, 3]. The synthesis of Janus and patchy particles remains a challenge. Many different techniques have been proposed in the literature [4], but still, breaking the symmetry at the surface of a colloid remains a hard task. The first approach consists in toposelective modifications. The very first example of anisotropic particles synthesis was described by de Gennes in 1992 [5], and consisted of glass microspheres around $50\ \mu\text{m}$ in diameter deposited on a solid substrate and embedded in a cellulose varnish of controllable thickness. The unprotected hemisphere was treated with a silane to render it hydrophobic. Since then, this method was applied to many colloids of different nature and size [6, 7, 8]. $1\ \mu\text{m}$ silica spheres could be immobilized in a photoresist layer, before an O_2 plasma etching was applied to remove partially the masking layer [6]. By controlling the time and the power of the plasma, it was possible to control the photoresist removal. Then gold and titanium nanolayers were deposited by electron-beam sputtering to modify the available surface. More recently, 15 nm platinum layer was deposited on silica particles by a simple vertical electron-beam method [7]. The resulting Janus colloids showed self-propelling motion under an electric field, and could be used as programmable colloidal shuttles to pick up, transfer and release cargo made of colloidal polymers of opposite surface charges. In a similar way, a monolayer of polymer spheres deposited on a substrate could be covered by a

32 nanometric gold layer by metal evaporation [9], or by metal sputtering [10]. Another toposelective technique is the microcontact printing, using a PDMS stamp allowing the transfer of molecules to the colloids, such as surfactants [11] or polyelectrolytes [12], and giving the possibility of multi-patches synthesis. Other techniques can be found in the literature such as lithography [13], microfluidics [14, 15], or Langmuir-Blodgett [16]. One limitation of all these methods is the low production yield, as only one monolayer of colloids is disposed at one interface. In that context the use of Pickering emulsions is a different promising approach which deals with much more particles by synthesis [17]. This method consists in preparing an O/W emulsion stabilized by colloids at moderate temperature (50 - 70°C) in order to have a liquid oil phase which solidifies during cooling at ambient temperature. Colloids are then immobilized at the O/W interface, allowing surface modification, before being released by dissolving the oil (in general paraffin). Granicks group first prepared dipolar silica particles with an aminosilane introduced in solution [18], or in vapor-phase [19]. They showed how the silica surface available was directly controlled by the contact angle at the O/W interface and thus by the surfactant concentration [20]. Other authors have then extended this technique to produce fluorinated silica [21], to decorate silica sheets with gold nanoparticles [22], or to create a TiO₂ layer on silica [23] for catalytic applications.

49 In this paper, the Pickering emulsion synthesis has been selected to produce one-patch inverse patchy colloids (IPCs), also called zwitterionic particles. These are anisotropic particles showing attractive interactions between the patch and the unpatched surface, while patch-patch and body-body interactions are repulsive. Such organic IPC have been for example proposed as drug delivery carriers [24, 25]. Our goal is to present a comparative study with experimental and numerical results on inorganic IPCs, in order to get a better understanding of their interactions, and to control their self-assembly in future applications. Some previous studies have already shown some comparisons between experimental suspensions and numerical simulations. One can cite Hong et al. for example, who have studied experimentally and numerically amphoteric Janus particles [26]. They have shown that aggregation forms compact aggregates, in which particles are oriented. Aggregation of two-patches IPCs has been also studied in details experimentally and numerically by Bianchi et al. [27, 28]

61 In this paper, first, the synthesis of one-patch IPCs of fluorescent silica will be presented. 62 Then different conditions of aggregation will be studied, by varying the size of the patch,

63 as well as the surface charges by varying the pH. The aggregates formed will be observed
64 directly in suspension by confocal microscopy. They will be compared to those obtained
65 using Brownian dynamics simulations.

66 **2. Materials and experimental methods**

67 *2.1. Chemicals*

68 Tetraethyl orthosilicate 98% (TEOS) and ammonium hydroxide NH_4OH 28% were pur-
69 chased from Acros Organic. The fluorescein isothiocyanate isomer I 90% (FITC) and the
70 3-aminopropyltriethoxysilane 99% (APTES) were purchased from Sigma-Aldrich. Absolute
71 ethanol and paraffin wax were provided by BDH Prolabo and Fisher Scientific, respectively.
72 Didodecyldimethylammonium bromide (DDAB) was supplied by Sigma Aldrich and cyclo-
73 hexane 99% was purchased from Alfa Aesar. All products were used as received.

74 *2.2. Particles synthesis*

75 In this study, home-made fluorescent silica particles are surface modified on only one part
76 by APTES to obtain amphoteric particles. For that, a Pickering emulsion route as proposed
77 by Hong *et al.* [18] is used. The different steps of synthesis are described in the following.

78 *Synthesis of fluorescent silica particles.* Fluorescent silica particles are synthesized according
79 to the protocol described in Reference 29. It is a modified Stöber synthesis consisting in
80 two steps. In a first one, monodispersed silica particles are synthesized by a classical Stöber
81 method which consists in the hydrolysis of TEOS in a mixture of ethanol, water and ammonia.
82 Then the fluorescent dye (here the FITC) previously bonded with the APTES is added. In a
83 second step, in order to minimize the presence of the dye on the particle surface, a silica shell
84 is grown by a dropwise addition of TEOS. Following the protocol presented in Reference 29,
85 fluorescent core-shell silica particles of around 600 nm are obtained.

86 *Pickering emulsions.* In order to modify partially the fluorescent silica particles, it is neces-
87 sary to hide a part of them. In this study, the particles are trapped in solid paraffin droplets
88 as proposed in Reference 18. For that, Pickering emulsions are prepared with paraffin wax,
89 water and silica particles [30]. To obtain partially hydrophobic silica, particles were modified
90 by DDAB. 140 mg of silica particles are thus introduced in 14 mL of osmosed water with the
91 DDAB. The suspensions are stirred at least 12 h to allow the DDAB adsorption on the silica

92 particles. As already shown in References [20, 30] the quantity of DDAB fix the contact angle
93 between the particle and the wax, and therefore the depth of penetration of silica particles in
94 the wax droplets. By modifying the quantity of DDAB, the surface available for modification
95 and therefore the patch size of the future IPCs can be tuned. In the following, three different
96 amounts of DDAB ($R = m_{DDAB}/m_{SiO_2}$ with m_{DDAB} the DDAB mass and m_{SiO_2} the silica
97 mass) will be used: $R = 5 \times 10^{-4}$, 1×10^{-3} and 1.5×10^{-3} . Pickering emulsions are then
98 prepared by adding 1 g of paraffin wax in the DDAB-silica suspension and by heating the
99 whole at 90°C to melt the wax. Emulsification is performed using Ultra Turrax stirring at
100 19000 rpm for 1 minute. Emulsions are then cooled down at room temperature to ensure
101 the solidification of the stabilized wax droplets. At this stage, silica particles are trapped on
102 solid wax droplets embedded in water.

103 *APTES grafting.* Naturally, silica particles are negatively charged in aqueous suspensions.
104 In order to have amphoteric particles, the not hidden part of particles will be modified by
105 grafting APTES. Generally, this grafting is performed in anhydrous solvents or in ethanol
106 based solvents in order to better control the rate of grafting [31, 32, 33]. Indeed, in water,
107 the APTES molecules can react with themselves limiting the grafting on silica [34, 35]. Many
108 anhydrous solvents dissolve the wax and thus can not be used in this study. Moreover, it
109 is known that ethanol can release silica particles from the solid wax droplets [20, 30] which
110 makes this solvent also not suitable for this study. That is why, even if grafting is not well
111 controlled, APTES will be grafted directly in water. Cuoq *et al.* have indeed shown that
112 a good rate of APTES grafting can be also obtained in water [34]. In this study, APTES
113 is added in the cold suspensions under stirring. Stirring is maintained over 20 minutes.
114 Then the emulsion is filtered on a Buchner funnel using 10 cm diameter Whatman Gr.541
115 filter paper and rinsed with deionized water. The solid wax droplets are then dried at room
116 temperature during 48 h.

117 *Wax removal.* The last stage of the synthesis consists in releasing the amphoteric particles
118 from the wax droplets. For that, wax is dissolved using cyclohexane. To try to isolate only
119 the synthesized IPCs, after dissolution, the mixture was centrifuged at 3000 rpm and powder
120 was obtained. However, it appeared that the obtained particles are mixed with small pieces of
121 wax. Moreover, the obtained particles are found hydrophobic because DDAB is still adsorbed
122 on them. Instead of centrifugation, a method using settling has been preferred. In order to

123 detach the DDAB, a HCl solution at pH 4 has been added in the beaker avoiding swirling
124 and stirred slowly over the night in order to avoid emulsification. After, the mixture is let to
125 settle in a separatory funnel. The two immiscible phases are observed and with time, colloids
126 settle from the upper cyclohexane phase to the lower HCl solution. In HCl, the particles
127 are aggregated which facilitates their sedimentation. At the end, the settled colloids in HCl
128 solution are less hydrophobic because they are not trapped at the interface. The aqueous
129 phase is isolated and centrifuged at 3000 rpm. Powder is then dispersed an other time 24 h
130 in HCL solution at pH 4 in order to remove all the remaining DDAB. After that, the powder
131 is centrifuged, rinsed 4 times in osmosed water and dried at 50°C during 16 h. It has been
132 verified that the obtained powders dispersed in water at a basic pH are not able to promote
133 the formation of a wax in water emulsion, which proves that the DDAB has been removed
134 from the particles.

135 *2.3. Characterization techniques*

136 Solid wax droplets are observed by scanning electron microscopy (SEM) on a SEM-Quanta
137 FEG - 450. To avoid charging effects, a thin film of platinum is deposited onto samples. As
138 proposed in References 20 and 30, SEM is used to determine the penetration depth of parti-
139 cles in the solid wax droplets. For that, the emulsions were rinsed by ethanol to remove the
140 silica from the wax. By comparing the diameter of the voids left in the wax and the silica
141 diameter, the penetration depth or the proportion of silica surface area taken up in the wax
142 is evaluated.

143 Zeta potential is measured using a Zetasizer Nano ZS from Malvern. For that, suspensions
144 of 0.3vol% are prepared in osmosed water and pH was adjusted with NaOH 0.1 M and HCl
145 0.1 M.

146 Aggregation is evaluated performing sedimentation tests. Suspensions are prepared with an
147 amount of 1vol% of silica particle at different pH. After preparation, the suspensions are
148 introduced into closed tubes and are allowed to settle. Analyses are performed after 24 h.
149 The cloudier the supernatant and the lower the sediment, the more stable the suspension.

150 Because silica particles are labeled by FITC, suspensions are observed by a confocal micro-
151 scope LSM880 from Zeiss. Suspensions are deposited between slide and slip cover. Images
152 are treated with ImageJ.

153

3. Simulation methods

Brownian dynamics simulations will be performed considering a 'raspberry' representation of IPCs. Details on this simulation technique can be found in Reference 36. To summarize, each colloid is represented by a hollow sphere decorated by 92 beads (see Figure 4), which will electrostatically interact with each other.

The interaction between IPCs is modeled here through a DLVO potential (Derjaguin, Landau, Verwey, Overbeek) [37, 38], which is the sum of two contributions: one attractive due to van der Waals interactions, and an electrostatic one due to the surface charges of the colloids. In this numerical study, the attractive interaction is applied as a central force and is expressed as:

$$V_{IJ}^{vdW} = -\frac{A_{IJ}}{6} \left[\frac{2a^2}{r_{IJ}^2 - (2a)^2} + \frac{2a^2}{r_{IJ}^2} + \ln \left(\frac{r_{IJ}^2 - (2a)^2}{r_{IJ}^2} \right) \right] \quad (1)$$

where A_{IJ} is the Hamaker constant, a is the radius of the IPCs and r_{IJ} is the center-to-center distance between IPCs I and J . Here $a = 300$ nm and $A_{IJ} = 4.6 \times 10^{-21}$ J [39].

The electrostatic interaction applied on an IPC is obtained by the sum of the electrostatic interactions applied on its beads, which are represented by a Hogg Healy Fuerstenau (HHF) potential [40]:

$$V_{ij}^{HHF_{bead}} = \pi\epsilon \frac{4a_b}{2} (\psi_i^2 + \psi_j^2) \left[\frac{2\psi_i\psi_j}{\psi_i^2 + \psi_j^2} \ln \left(\frac{1 + \exp(-\kappa h_{ij})}{1 - \exp(-\kappa h_{ij})} \right) + \ln(1 - \exp(-2\kappa h_{ij})) \right] \quad (2)$$

where ψ_i is the surface potential of bead i , h_{ij} is the surface-to-surface distance between beads i and j , κ the inverse of Debye length ($\kappa = 10^8$ m⁻¹) and a_b is the bead radius (here $a_b = 66.58$ nm). As proposed in Reference 36, a factor 4 is used in the HHF expression, which allows to reproduce the behavior of suspensions, where heteroaggregation occurs. To avoid interpenetration of IPCs at the contact, the attractive interactions are cut at $-14k_B T$ and a linear repulsive potential is introduced as a central interaction when IPCs are in contact.

Both the translational and the rotational motions of IPCs are introduced in Brownian dynamics simulations. Simulations are performed with 1500 IPCs in a cubic box with periodic conditions. A volume fraction of 3vol% is used. Simulations have been performed with a time step of 10^{-7} s. Results are analyzed at 10 s. Because of the large number of beads used in these simulations, simulations have been performed thanks to a parallelized home-made code developed for calculations on GPU (Graphics Processing Unit) based on the strategies presented in Reference 41.

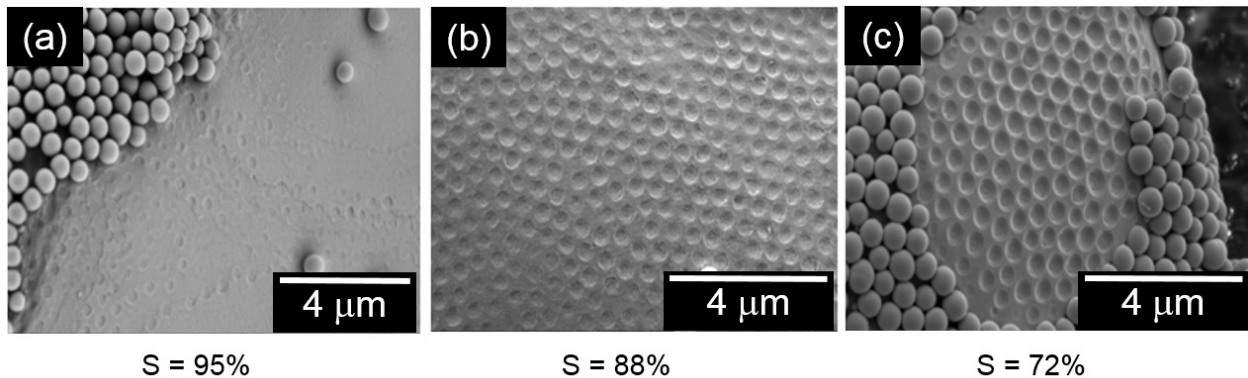


Figure 1: SEM images of solid wax/silica droplets rinsed with ethanol at various concentrations of DDAB: (a) $R = 5 \times 10^{-4}$, (b) $R = 1 \times 10^{-3}$ and (c) $R = 1.5 \times 10^{-3}$. S represents the proportion of silica surface area that will be modified by APTES.

182 4. Results and discussion

183 4.1. Characterization of the synthesized one-patch IPCs

184 As already mentioned, the quantity of DDAB used to prepare the wax-in-water Pickering-
 185 ing emulsion determine the depth of silica penetration in the wax and thus the surface that
 186 can be modified by APTES. To quantify this surface, the cold emulsions have been rinsed
 187 by ethanol in order to remove some silica particles from the wax. The obtained droplets,
 188 observed by SEM, are shown in Figure 1. By measuring the diameter of the indentations,
 189 the depth of penetration and therefore the surface area accessible for modification have been
 190 determined. Modified surface area proportions of $S = 95\%$, $S = 88\%$ and $S = 72\%$ have
 191 been obtained with the DDAB ratios $R = 5 \times 10^{-4}$, 1×10^{-3} and 1.5×10^{-3} , respectively.
 192 In order to check that the APTES is grafted on the silica during the synthesis, zeta potential
 193 measurements have been performed on the synthesized IPCs as reported in Figure 2a. In
 194 comparison, the zeta potential measured for the raw silica particles ($S=0\%$) as well as the
 195 zeta potential of silica particles whose surface is totally grafted by APTES ($S=100\%$) are
 196 also reported. It can be observed that the raw silica have a negative zeta potential over the
 197 whole pH range whereas the totally grafted silica particles show an isoelectric point around
 198 $\text{pH}=7.5$. Below this pH the modified silica particles are positively charged, due to the pro-
 199 tonation of the NH_2 groups of APTES, whereas above this pH they are negatively charged.
 200 For the IPCs, zeta potential curves are found in between the curves for $S=0\%$ and $S=100\%$,
 201 which is in agreement with partial particle coverage by APTES. Moreover, the greater the

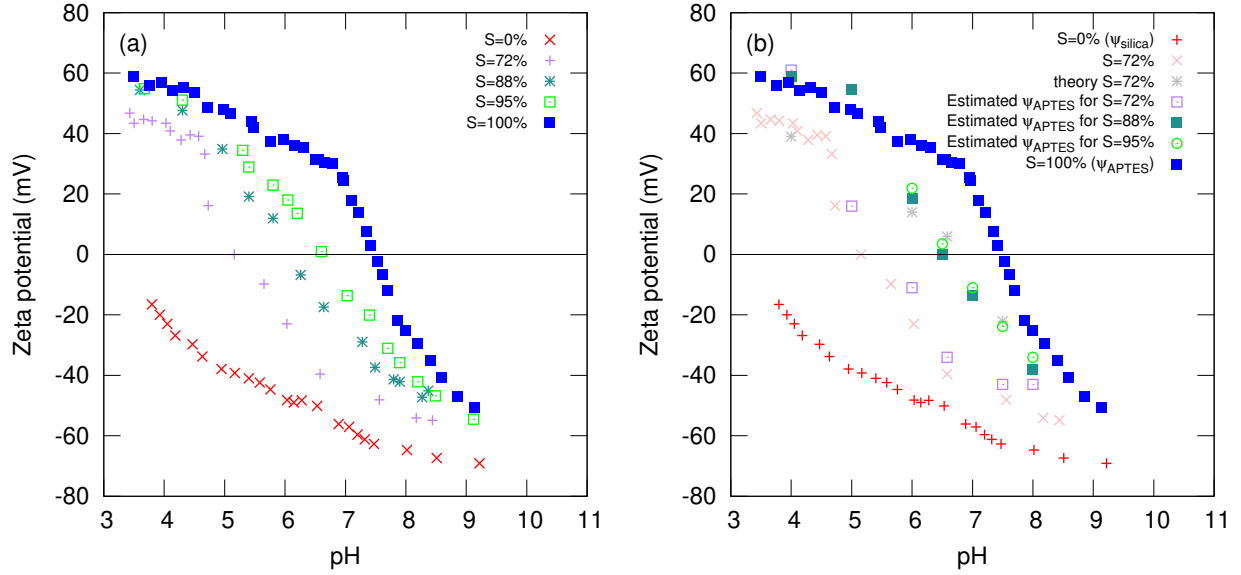


Figure 2: (a) Evolution of the experimental zeta potential of IPCs as a function of the pH. By comparison, results obtained with raw silica particle ($S = 0\%$) and silica fully modified ($S = 100\%$) are reported. (b) Calculated surface potentials for $S = 72\%$ considering that the patch reacts as the raw silica and the unpatched part as the full APTES modified silica (theory $S=72\%$). Calculated surface potentials of the APTES modified parts of IPCs for $S=72\%$ (Estimated ψ_{APTES} for $S=72\%$), $S=88\%$ (Estimated ψ_{APTES} for $S=88\%$) and $S=95\%$ (Estimated ψ_{APTES} for $S=95\%$).

202 proportion of modified surface area, the closer the curve is to the case $S=100\%$.

203

204 To understand the behavior of amphoteric particle suspensions and for their simulation,
 205 it is important to know the electric potential at the surface of each part of the particles
 206 as a function of the pH: the unmodified part called “silica” and the modified part called
 207 “APTES”. We discuss this point in the following.

208 A reasonable hypothesis would be to consider that the potential of the unmodified part is that
 209 of the initial silica, $\psi_{silica} = \psi_{0\%}$ (the potential measured for $S = 0\%$), and that the potential
 210 of the modified part is that measured for the completely modified silica, $\psi_{APTES} = \psi_{100\%}$
 211 (the potential measured for $S = 100\%$). At this point, at $\text{pH}=7.5$, we would expect that
 212 the suspension would not be stable since $\psi_{100\%}$ is close to 0, but sedimentation tests show
 213 on the contrary that the suspension is stable at this pH. On the other hand, knowing the
 214 surface potential, the following formula allows us to go up to the corresponding surface charge

215 quantity [42]:

$$Z = 4\pi\epsilon \frac{k_B T}{ze^2} \kappa a^2 \left[2 \sinh \left(\frac{1}{2} \frac{ze\psi}{k_B T} \right) + \frac{4}{\kappa a} \tanh \left(\frac{1}{4} \frac{ze\psi}{k_B T} \right) \right], \quad (3)$$

216 where e is the elementary charge and z the electrolyte valence (here $z=1$). Thus, by using
217 the surface proportion at $\psi_{0\%}$ and that at $\psi_{100\%}$, we can estimate the number of charges of
218 the unmodified part Z_{silica} and that of the modified part Z_{APTES} , i.e., by summing up the
219 total number of charges Z_T , and thus, by adjustment using equation 3, a theoretical surface
220 potential ψ_{theo} . This estimate was made for IPCs at $S = 72\%$ and the result is shown in Fig-
221 ure 2b. It is clearly observed that the calculated curve does not correspond to the measured
222 one.

223 These two disagreements could be explained by a grafting rate of APTES, while the parti-
224 cles are embedded in the wax, lower than that obtained for completely uncovered particles
225 ($S = 100\%$), without the wax. As already mentioned, the APTES grafting in water is diffi-
226 cult to control because of its self-reaction and moreover, in case of Pickering emulsions, the
227 presence of different phases can also affect this grafting. This would mean that ψ_{APTES} is
228 different from $\psi_{100\%}$ and lower.

229 Another hypothesis for estimating ψ_{APTES} is to deduce the total number of charges Z_T from
230 the measured zeta potential, estimate the number of charges of the unmodified part Z_{silica}
231 from the proportion of unmodified area and $\psi_{0\%}$ (ψ_{silica} is assumed to be equal to $\psi_{0\%}$),
232 deduce Z_{APTES} from this and go back to ψ_{APTES} by fitting with equation 3.

233 These estimations, shown in Figure 2b, reveal that the surface potential of modified part may
234 be lower than ψ_{APTES} in a pH range comprised in [5-7.5] for the case $S = 72\%$ and in a pH
235 range of [6-7.5] for the cases $S = 88\%$ and 95% . For $S = 72\%$, the PCN of the modified part
236 is estimated at 5.5 and thus at pH 7.5, both parts of particles may be negatively charged
237 and thus suspension must be stable, which is in agreement with the previous sedimentation
238 tests.

239 In the following, for each IPC, aggregation will be analyzed for three different pH. The first
240 one, pH_a , corresponds to the case where the APTES modified surface is positively charged
241 and the unmodified part is negatively charged. The second one, pH_n , corresponds to a pH
242 where the APTES surface modified has surface potential around 0. And the third one, pH_b ,
243 corresponds to the case where both parts of IPCs are negatively charged. In the following,
244 a pH in the range [4.5-5] is chosen as pH_a and a pH in the range [7.5-8] as pH_b whatever

245 the size of the modified surface. Because of the difficulty to evaluate precisely the PCN of
246 the modified part due the rough estimations used in the model as well as the experimental
247 difficulties to obtain precise measurements of zeta potential near the isoelectric point, pH_n
248 is chosen in a larger range [5.5-6.5]. At pH_n it is verified by sedimentation tests that the
249 suspension aggregate and that, for higher pH, it becomes stable.

250

251 *4.2. Study of one-patch IPC aggregation*

252 Sedimentation tests are performed with colloidal suspensions prepared with a volume
253 fraction of 1vol% for the different pH reported in the previous section. Figure 3 shows the
254 results obtained at 24 h. Moreover, because particles are labeled with FITC, the suspensions
255 are observed by confocal microscopy as also shown in Figure 3.

256

257 For pH_b , it is observed that all the suspensions are stable. The sediments are low and
258 only individual particles are observed by microscopy. According to Figure 2, at pH_b both
259 parts of IPCs are negatively charged and thus aggregation of IPCs is unlikely.

260 For pH_n , the raw silica is stable and negatively charged. However, this pH is near the
261 isoelectric point of the APTES part of the IPCs, which aggregate because of the van der
262 Waals interactions. For IPC suspensions, higher sediment is observed in the sedimentation
263 tubes and aggregates are clearly observed by confocal microscopy whatever the patch size.

264 As for pH_a , the totally modified particles (S=100%) and the raw silica particles (S=0%) are
265 stable. Nevertheless, in case S=100%, particles are positively charged and in case S=0%
266 particles are negatively charged (see Figure 2). For IPC suspensions at pH_a , the sediments
267 are slightly lower than those obtained at pH_n . However they are higher than the sediments
268 obtained at pH_b , which is explained by an aggregation of IPCs in suspension. Aggregates
269 are indeed observed by confocal microscopy. At this pH, the patch and the unpatched parts
270 of IPCs are oppositely charged and aggregation can be explained by the attractions between
271 the two parts of IPCs. For the largest patch (S=72%), confocal microscopy observations
272 reveal that aggregates are compact (see Figure 3). To better understand the aggregation
273 mechanisms in IPC suspensions, Brownian dynamics simulations have been used.

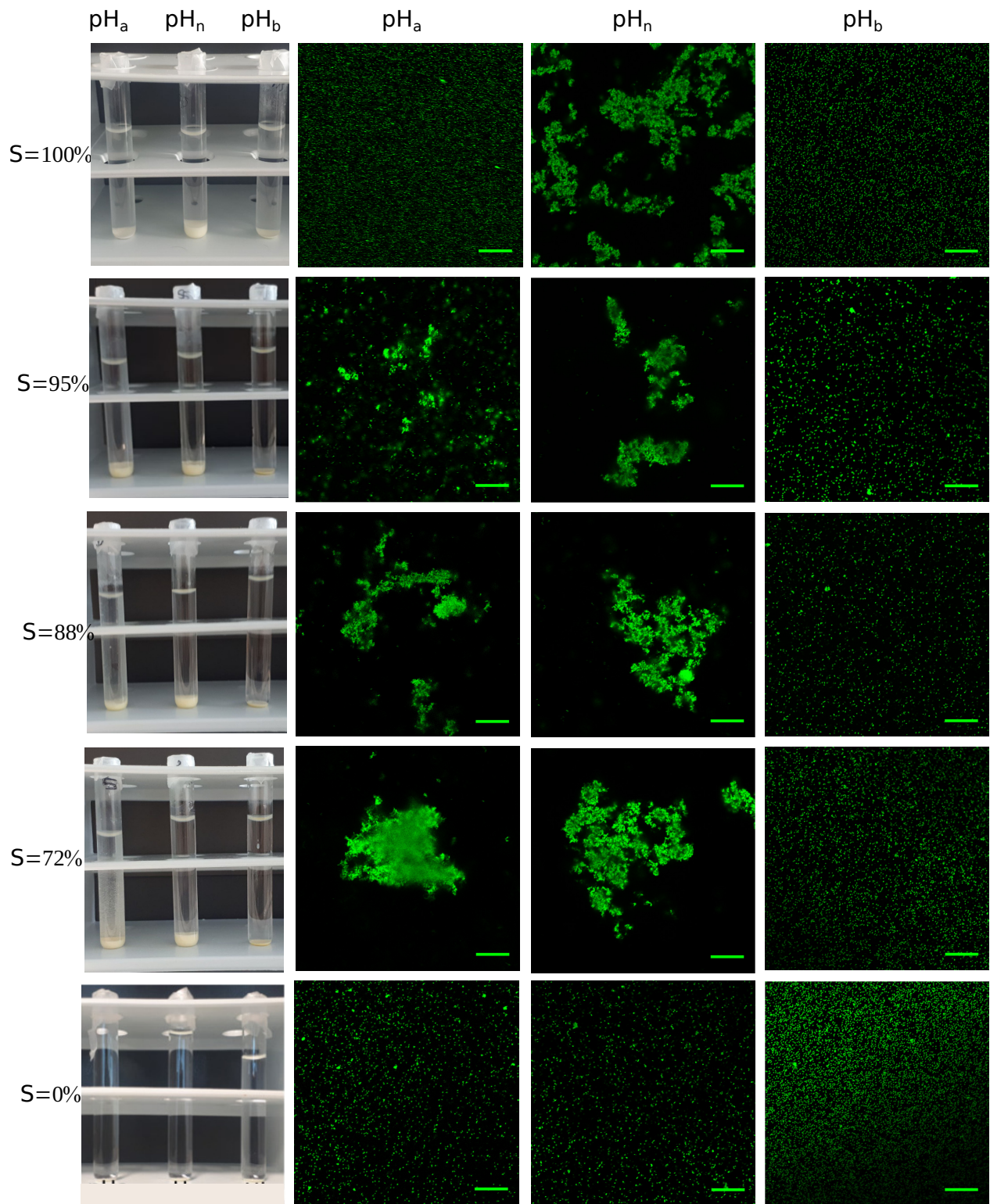


Figure 3: Picture of sedimentation test and corresponding confocal microscopy images for the different pH as a function of the size of the modified part of IPCs (S). The scale bar is for $20\ \mu\text{m}$.

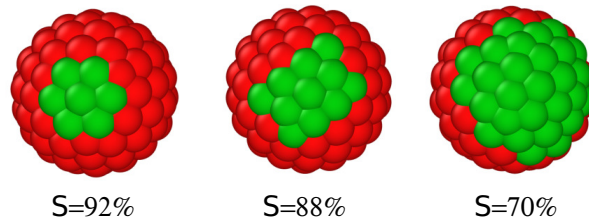


Figure 4: Snapshots of IPCs used in Brownian dynamics simulations with their proportion of red surface area (corresponding to the APTES modified part).

	S=92%		S=88%		S=70%	
	ψ_{silica} (mV)	ψ_{APTES} (mV)	ψ_{silica} (mV)	ψ_{APTES} (mV)	ψ_{silica} (mV)	ψ_{APTES} (mV)
pH _a	-40	50	-40	50	-40	20
pH _n	-60	0	-60	0	-50	0
pH _b	-65	-25	-65	-35	-65	-45

Table 1: Summary of the different values of surface potentials (ψ) used in simulations.

274 4.3. Brownian dynamics simulations of one-patch IPC aggregation

275 Figure 4 shows the one patch IPCs used in simulations. The green part corresponds to the
 276 unmodified part of silica particle and the red part corresponds to the APTES modified part.
 277 Patches are defined in order to fit with the experimental patch sizes. The surface potentials
 278 used in the HHF potential (Equation 2) are assimilated here to the surface potential of the
 279 raw silica (ψ_{silica}) for the unmodified part and to the estimated APTES surface potential
 280 (ψ_{APTES}) for the modified part. Table 1 summarizes the values of surface potential used in
 281 simulations.

282 For a comparison, a simulation has also been performed with particles without patch,
 283 which interact only via the van der Waals attraction (case where $S = 100\%$ at pH_n). Fig-
 284 ures 5 and 6 show the results of simulations at $t = 10$ s for the different patch sizes. The
 285 aggregation kinetics as well as the evolution of the aggregate shape as a function of time are
 286 shown in Figure 7.

287

288 At pH_b, for all patch sizes, no aggregation is observed in the simulations in agreement
 289 with the experimental observations. Both parts of IPC are negatively charged. Particles
 290 repel each other leading to stable suspensions.

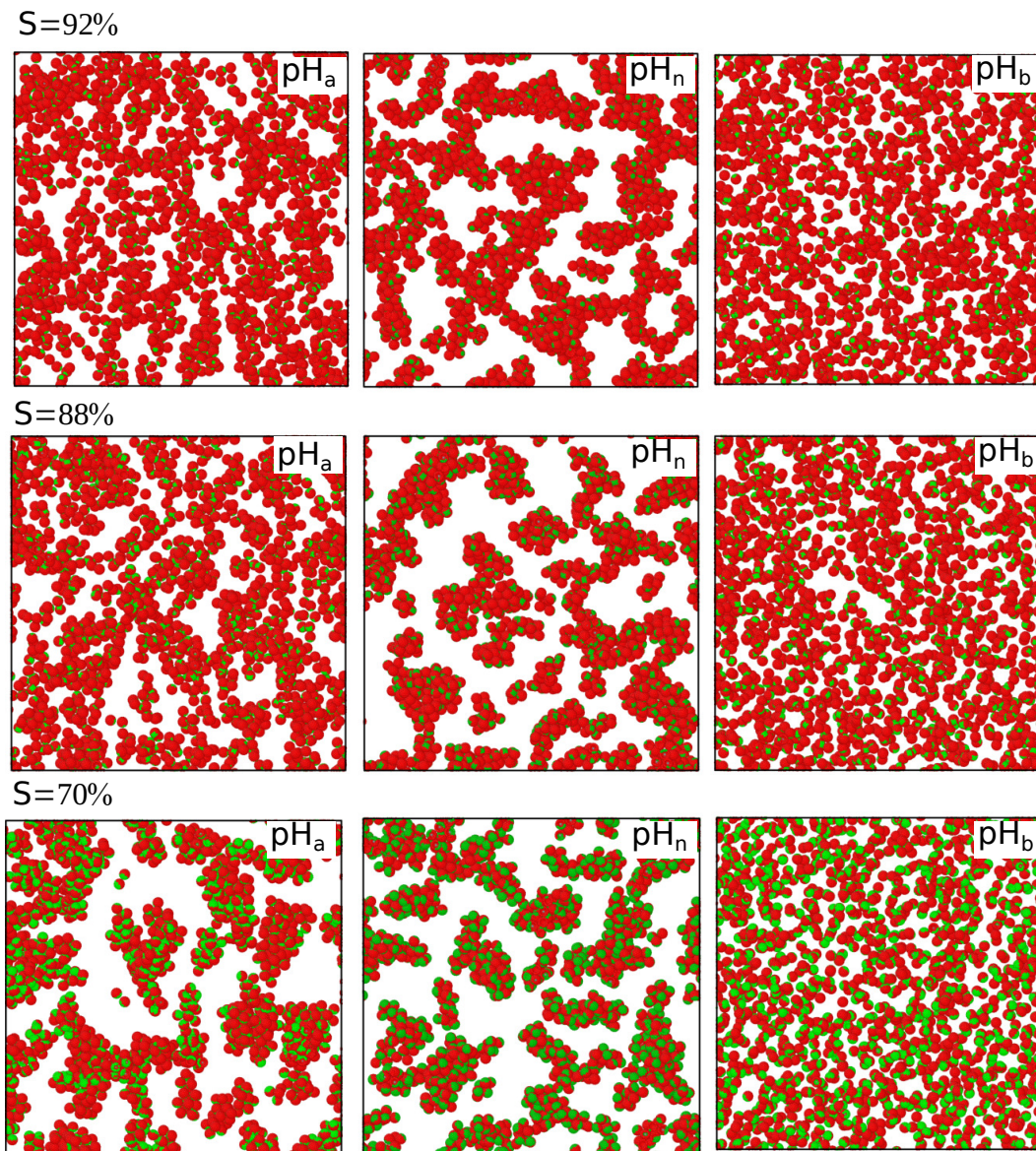


Figure 5: Snapshots of Brownian dynamics simulations obtained at $t = 10$ s for the different pH as a function of the size of the unpatched part (APTES modified).

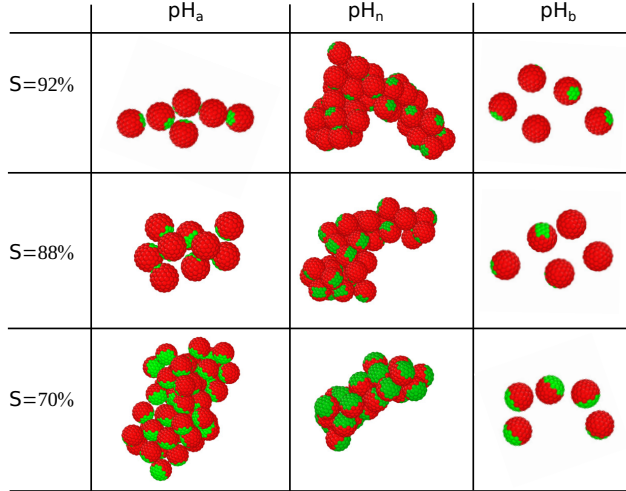


Figure 6: Snapshots of isolated aggregates extracted from the Brownian dynamics simulations performed with different pH and different sizes of the unpatched part (S). At pH_b no aggregate were formed.

291 At pH_a, for which the two parts of IPCs are oppositely charged, aggregation is observed
292 regardless of S . Aggregates are formed by contacts between the modified and the unmodified
293 parts of particles, which are oppositely charged (see Figure 6). However aggregate size and
294 shape differ depending on S . Figure 7a shows the evolution of the number of aggregates
295 composed of at least two IPCs as a function of time. As already observed in Reference [36],
296 the aggregation kinetics slows down when S increases. Thus, at the end of simulations, when
297 S increases, the aggregate size decreases. This observation is in good agreement with the
298 confocal microscopy pictures reported in Figure 3. To characterize the aggregate structure,
299 the coordination number of aggregated particles is plotted in Figure 7c. For all the values of
300 S , at the beginning of simulations, this number is equal to 1. At this stage, it is observed in
301 Figure 7a that the number of aggregates increases which corresponds to the dimer formation
302 regime and thus the coordination number is equal to one. Then, when the number of aggre-
303 gates decreases due to their coalescence, the coordination number increases. For $S = 70\%$,
304 this number is around 6 at $t = 10$ s, which corresponds to quite compact aggregates as ob-
305 served in Figure 6. However, for the smaller values of S , this number is smaller, around 2
306 or 3 for $S = 92\%$ and $S = 88\%$ respectively. In this case the aggregates are more linear
307 (see Figure 6). To characterize the shape of aggregates, the asphericity parameter has been
308 calculated, according to [43, 44]:

$$A_s = \frac{(\lambda_1 - \lambda_2)^2 + (\lambda_2 - \lambda_3)^2 + (\lambda_3 - \lambda_1)^2}{2(\lambda_1 + \lambda_2 + \lambda_3)^2} \quad (4)$$

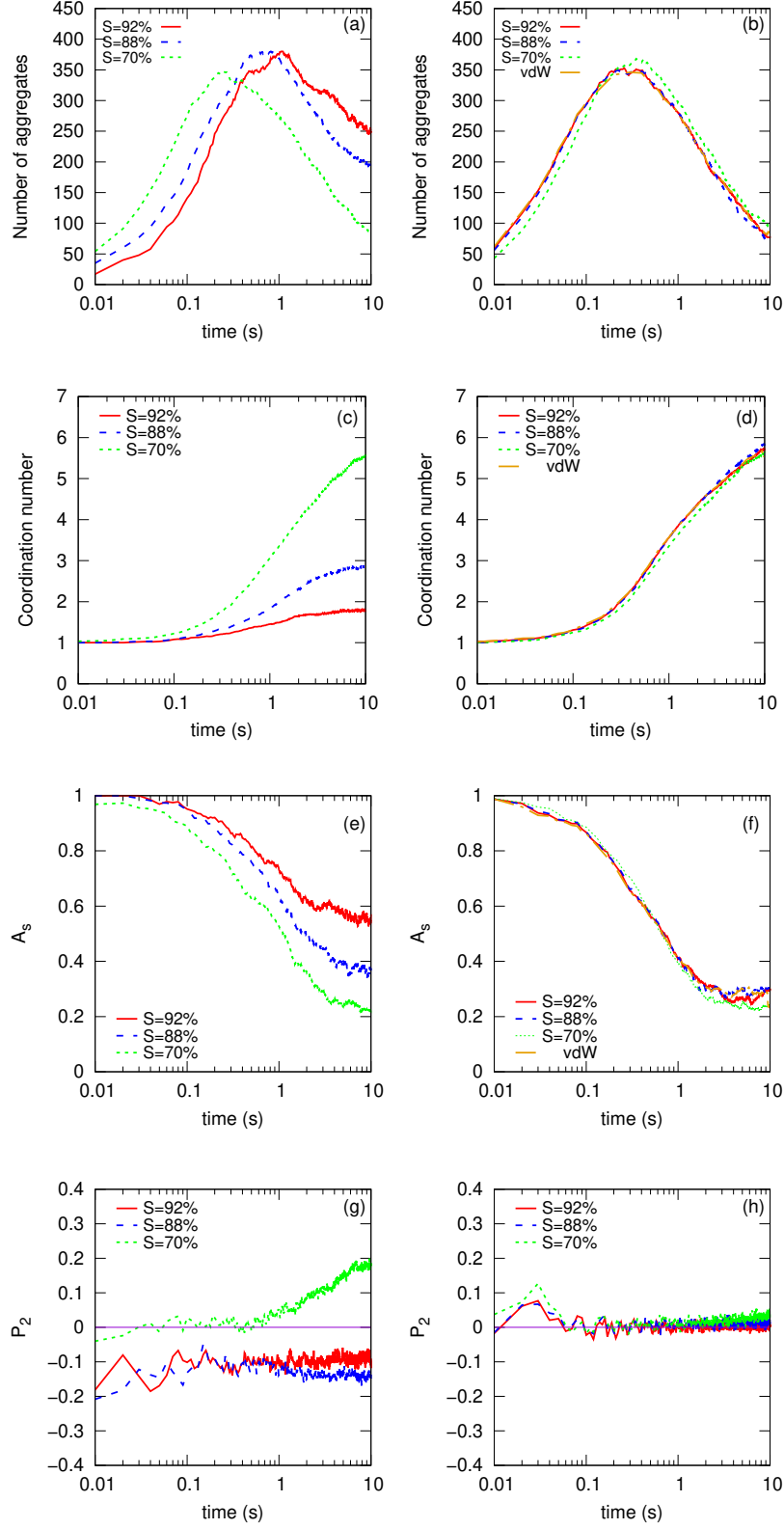


Figure 7: Characterization of the aggregation in the Brownian dynamics simulations performed for different sizes of the silica modified part ($S = 92\%$, $S = 88\%$ and $S = 70\%$) and for uniform particles interacting only via van der Waals attractions ($S = 100\%$ at pH_n): number of aggregates for pH_a (a) and pH_n (b); evolution of the coordination number for pH_a (c) and pH_n (d); evolution of the asphericity parameter (A_s) for pH_a (e) and pH_n (f) and evolution of P_2 for pH_a (g) and pH_n (h).

309 with λ_1 , λ_2 and λ_3 ($\lambda_1 \geq \lambda_2 \geq \lambda_3$) the eigenvalues of the radius of gyration tensor defined as:

$$T_{\alpha\beta} = \frac{1}{N} \sum_{I=1}^N (r_{\alpha,I} - r_{\alpha,center}) (r_{\beta,I} - r_{\beta,center}) \quad (5)$$

310 $r_{\alpha,I}$ is the coordinate of the particle I and $r_{\alpha,center}$ the center of mass coordinate of the
 311 aggregate containing I . α , β represent the Cartesian coordinates (x, y or z), and N is the
 312 number of particles contained in the aggregate. Asphericity is null for a sphere and equal to
 313 one for a rod-like structure. The evolution of A_s is reported in Figure 7e. At the beginning
 314 of simulations, whatever S , $A_s = 1$, which is explained by the dimers formed at this stage
 315 of aggregation. At $t = 10$ s, A_s is smaller when S decreases and therefore aggregates are
 316 more spherical. Fractal dimensions (D_f) obtained by plotting the number of particles of the
 317 aggregate as a function of its radius of gyration confirm this observation. $D_f = 1.34 \pm 0.03$,
 318 1.54 ± 0.03 and 1.96 ± 0.04 have indeed been found for $S = 92\%$, 88% and 70% respectively.
 319 An other important parameter for aggregated patchy particles is their mutual orientation in
 320 the aggregate. To characterize it, the nematic order parameter defined by the second-order
 321 Legendre polynomial is used [45, 46]:

$$\langle P_2 \rangle = \left\langle \frac{3 \frac{1}{N_I} \sum_{J=1}^{N_I} (\mathbf{u}_I \cdot \mathbf{u}_J)^2 - 1}{2} \right\rangle \quad (6)$$

322 with N_I the number of neighbors of particle I and \mathbf{u}_I the unit vector of particle I directed
 323 from the center of the particle to the center of its patch (here the non-modified part of par-
 324 ticle). Values of $\langle P_2 \rangle$ are in the range $[-0.5; 1]$ [47, 48]. When all vectors of neighboring
 325 particles are perfectly aligned, $\langle P_2 \rangle$ is equal to 1. If all the neighboring particles are
 326 randomly oriented, $\langle P_2 \rangle$ is null. And a value of -0.5 corresponds to an orthogonal orien-
 327 tation. Figure 7g shows the evolution of $\langle P_2 \rangle$ as a function of time. Values of $\langle P_2 \rangle$
 328 are small, which indicates that IPCs are poorly oriented in the aggregates. However it is not
 329 zero. When $S = 70\%$, $\langle P_2 \rangle$ becomes positive which corresponds to a beginning of align-
 330 ment of particles in the same direction. However, for the smaller S , $\langle P_2 \rangle$ is negative, the
 331 unmodified parts are rather orthogonally oriented. All these observations are in agreement
 332 with previous observations from the literature [36, 49, 50].

333 At pH_n , simulations show a strong aggregation of particles whatever S , which is in agreement
 334 with the experimental observations (see Figure 3). Contacts in aggregates are obtained essen-
 335 tially between the modified parts or between the modified and unmodified parts. At this pH,

336 there is not much difference in the aggregation kinetics for the different S (see Figure 7b). It
 337 is also observed that this kinetics is similar to the kinetics observed in the simulation where
 338 particles only experience van der Waals attraction. At this pH, the modified parts of IPCs
 339 are not charged and aggregation is mainly due to van der Waals interactions between them.
 340 For all values of S , aggregates are compact with a coordination number around 6, and they
 341 have an asphericity around 0.25 (see Figures 7d and 7f). Fractal dimensions are found at
 342 $D_f = 1.74 \pm 0.04$, 1.72 ± 0.04 and 1.81 ± 0.04 for $S = 92\%$, 88% and 70% respectively. It is also
 343 observed that particles are randomly oriented in the aggregates unlike at pH_a (see Figures 7h
 344 and 6).

345

346 In Figure 3, for $S = 72\%$ at pH_a , aggregates seem more compact compared to the ag-
 347 gregates obtained with $S = 100\%$ at pH_n , which is the more common aggregation in oxide
 348 suspensions. To see if the simulations could provide an explanation for this observation,
 349 complementary calculations have been performed until $t = 20$ s for $S = 70\%$ at pH_a and pH_n
 350 and for particles interacting only through van der Waals attractions (similar to $S = 100\%$
 351 at pH_n). Snapshots of the simulations obtained at $t = 20$ s as well as the evolution of A_s
 352 are shown in Figure 8. After 10 s, it appears that A_s slightly increases in simulations where
 353 particles interact only with van der Waals interactions contrary to the IPCs. In this case,
 354 aggregates are thus more elongated. Fractal dimensions measured at $D_f = 1.89 \pm 0.06$,
 355 1.73 ± 0.05 and 1.63 ± 0.05 for pH_a , pH_b and for the van der Waals interactions respectively,
 356 confirm this observation. From previous works, it is known that the shape of aggregates is
 357 explained by the competition between the kinetics of aggregate coalescence and the kinetics
 358 of aggregate reorganization [51]. Since the kinetics of aggregate coalescence is similar in the
 359 three simulations (at $t = 20$ s, 54, 55 and 54 aggregates are found for pH_a , pH_b and for the
 360 van der Waals interactions respectively), this difference should be explained by the aggregate
 361 reorganization. Reorganization of the aggregates is indeed expected in order to maximize the
 362 number of contacts between the attractive parts of particles, which minimizes the potential
 363 energy and gives compact configurations. The reorganization kinetics has been assessed by
 364 following the reorganization of an isolated aggregate obtained just after the coalescence of
 365 two small aggregates (see Figure 9). The reorganization has been characterized by the as-
 366 phericity A_s and the mean coordination number of aggregated particles as a function of time

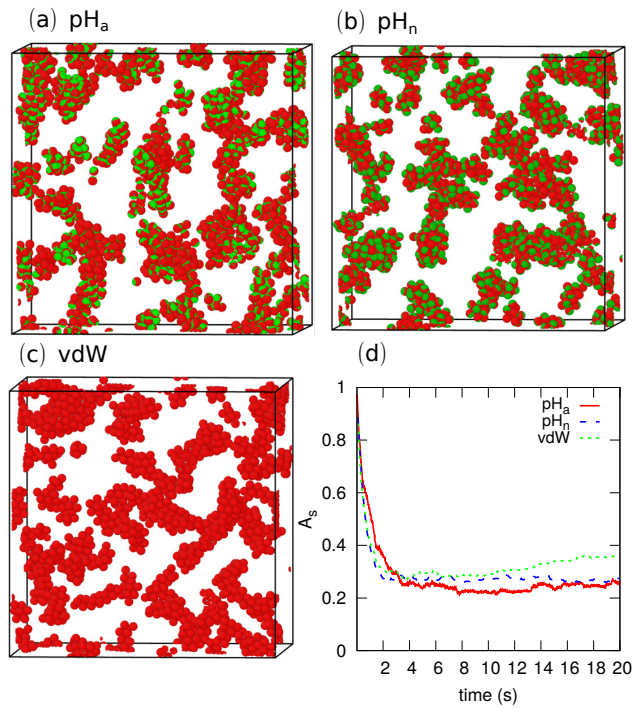


Figure 8: Snapshots of simulations obtained at $t = 20$ s: (a) $S = 70\%$ at pH_a , (b) $S = 70\%$ at pH_n and (c) $S = 100\%$ at pH_n (particles interact only via van der Waals interactions). (d) Evolution of the asphericity as a function of time in these simulations: pH_a ($S = 70\%$ at pH_a), pH_n ($S = 70\%$ at pH_n) and vdW ($S = 100\%$ at pH_n).

(see Figure 10). It should be noted that, after 1 s, asphericity and coordination no longer evolves in the case of the aggregate of particles interacting via van der Waals, whereas for the IPCs a continuous reorganization of the aggregates is observed. Indeed, for IPCs, A_s as well as the averaged coordination number vary all along the simulations. The coordination number sometimes decreases, which corresponds to the dissociation of particles and promotes the aggregate reorganization. Nevertheless, in our simulations, the coordination overall increases reflecting the aggregate reorganization in a more compact shape. Bochicchio *et al.* have shown that long dissociation times (e.g. ≈ 150 s) prevent from the aggregate reorganization leading to “branched” aggregates, whereas short ones (e.g. ≈ 0.3 s) allow an important aggregate reorganization leading to compact, even crystallized aggregates in Brownian dynamics simulations [52]. In previous simulations, the dissociation time of two aggregated patchy particles with S in the range [60;70]% was measured at around 3 s [36]. This value is low and may explain an important aggregate reorganization in the IPC simulations. The relatively easy dissociation of the IPCs is due to repulsions between some parts of the IPCs. Thus, in the present simulations, when particles interact only via van der Waals interactions, the reorganization is slow and this leads to elongated aggregates. On the contrary, IPC aggregates can be reorganized much more easily to maximize the contact number between the attractive parts, leading to more compact aggregates.

5. Conclusion

One patch silica-based IPCs have been synthesized with different patch sizes. Their aggregation in suspension has been studied both experimentally and numerically at different pH. A good agreement is obtained between the simulation results and the experimental characterizations. For pH where both parts of IPCs are negatively charged (pH_b), no aggregation is observed. At acidic pH, where the two parts of the particles are oppositely charged (pH_a), aggregation is observed in all cases. The size of the patch has a strong influence on the aggregate structures. The smaller the patch, the more the aggregates are elongated. For the patch sizes studied here, a slight organization of the particles is found in the aggregates. All of these observations are consistent with the findings in the literature [49, 50]. For pH where the modified part of the particles is weakly charged (pH_n), a strong aggregation is obtained whatever the size of this part. Aggregation is mainly due to van der Waals attractions and no

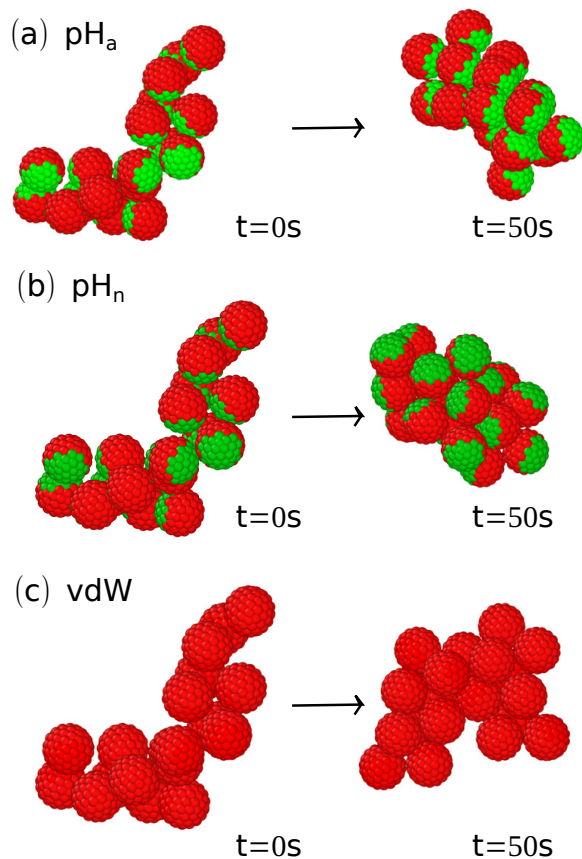


Figure 9: Snapshots of simulations performed on an isolated aggregate: (a) $S = 70\%$ at pH_a , (b) $S = 70\%$ at pH_n and (c) $S = 100\%$ at pH_n (particles interact only via van der Waals interactions).

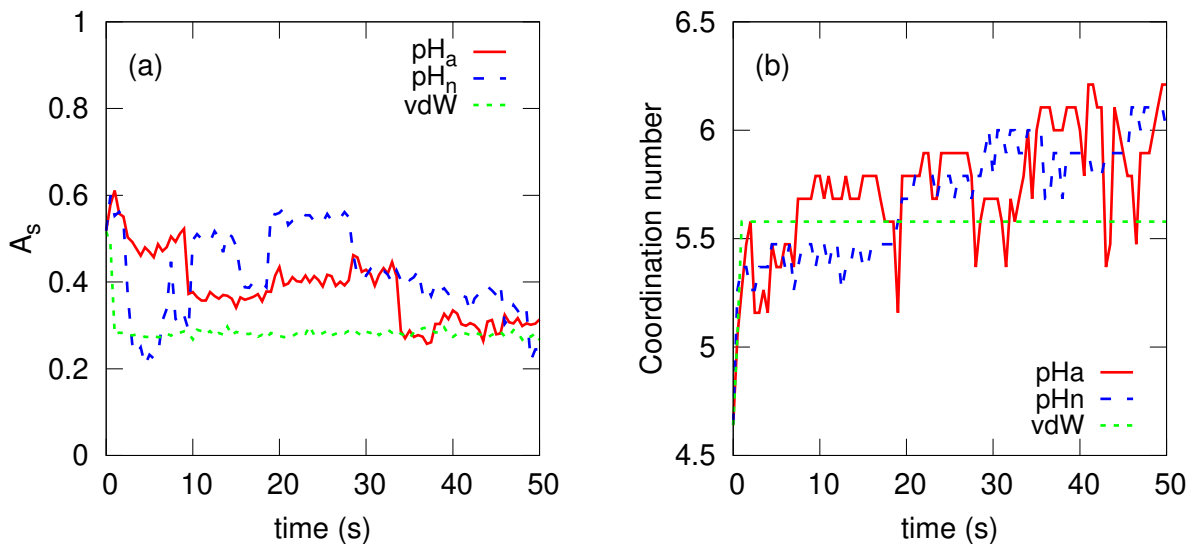


Figure 10: Evolution of the asphericity (a) and of the averaged coordination number (b) as a function of time in simulations performed on an isolated aggregate: pH_a ($S = 70\%$ at pH_a), pH_n ($S = 70\%$ at pH_n) and vdW ($S = 100\%$ at pH_n).

397 organization is found in the aggregates. It is also observed experimentally, that the largest
398 patch size leads to compact aggregates especially at acidic pH. Numerically, this may be
399 explained by an important reorganization of the aggregates due to the presence of repulsive
400 parts on the colloid surface.

401 All these results show that the aggregation of the synthesized silica based amphoteric parti-
402 cles can be tuned by modifying both the proportion of the modified part of the particles and
403 the pH. Such particles can be used to obtain either elongated or compact aggregates in
404 which the particles may have a preferential orientation, which makes them promising to build
405 new ceramic materials.

406 **Acknowledgments**

407 The authors thank the Région Nouvelle-Aquitaine for its financial support. The authors
408 thank also CALI and its team for providing the computational facilities (CALI has been
409 financed by the region Limousin, the institutes XLIM, IPAM, GEIST, and the University of
410 Limoges). Figures 4, 5, 6, 8, 9 have been obtained by Ovito [53].

411 [1] M. Zrinyi, Z. Hrvlgyi (Eds.), *From Colloids to Nanotechnology*, 2004th Edition, Springer,
412 2004.

413 [2] F. Li, D. P. Josephson, A. Stein, *Colloidal assembly: The road from particles to colloidal*
414 *molecules and crystals*, *Angewandte Chemie International Edition* 50 (2) (2011) 360–388.

415 [3] D. Morpew, D. Chakrabarti, *Clusters of anisotropic colloidal particles: From colloidal*
416 *molecules to supracolloidal structures*, *Curr. Opin. Colloid Interface Sci.* 30 (2017) 70 –
417 80.

418 [4] A. Perro, S. Reculosa, S. Ravaine, E. Bourgeat-Lami, E. Duguet, *Design and synthesis*
419 *of Janus micro- and nanoparticles*, *Journal of Materials Chemistry* 15 (35-36) (2005)
420 3745–3760. doi:10.1039/B505099E.

421 [5] P.-G. de Gennes, *Soft Matter (Nobel Lecture)*, *Angewandte Chemie International Edi-*
422 *tion in English* 31 (7) (1992) 842–845. doi:10.1002/anie.199208421.

- 423 [6] Z. Bao, L. Chen, M. Weldon, E. Chandross, O. Cherniavskaya, Y. Dai, J.-H. Tok, Toward
424 controllable self-assembly of microstructures: selective functionalization and fabrication
425 of patterned spheres, *Chem. Mater.* 14 (2002) 24–26. doi:10.1021/cm010739n.
- 426 [7] A. F. Demirörs, M. T. Akan, E. Poloni, A. R. Studart, Active cargo transport with janus
427 colloidal shuttles using electric and magnetic fields, *Soft Matter* 14 (2018) 4741–4749.
- 428 [8] J. Ji, M. Fuji, H. Watanabe, T. Shirai, Partially functionalized janus ZnO spheres
429 prepared by protecting mask techniques, *Colloids Surf., A* 393 (2012) 6 – 10.
430 doi:<https://doi.org/10.1016/j.colsurfa.2011.09.042>.
- 431 [9] H. Takei, N. Shimizu, Gradient Sensitive Microscopic Probes Prepared by Gold Evap-
432 oration and Chemisorption on Latex Spheres, *Langmuir* 13 (7) (1997) 1865–1868.
433 doi:10.1021/la9621067.
- 434 [10] D. Suzuki, H. Kawaguchi, Janus particles with a functional gold surface for control of
435 surface plasmon resonance, *Colloid and Polymer Science* 284 (12) (2006) 1471–1476.
436 doi:10.1007/s00396-006-1524-5.
- 437 [11] O. Cayre, V. N. Paunov, O. D. Velev, Fabrication of dipolar colloid particles by micro-
438 contact printing, *Chem. Commun.* (2003) 2296–2297doi:10.1039/B307296G.
439 URL <http://dx.doi.org/10.1039/B307296G>
- 440 [12] F. N. Mehr, D. Grigoriev, N. Pureskiy, A. Bker, Mono-patchy zwitterionic microcolloids
441 as building blocks for ph-controlled self-assembly, *Soft Matter* 15 (2019) 2430–2438.
442 doi:10.1039/C8SM02151A.
- 443 [13] A. B. Pawar, I. Kretzschmar, Fabrication, Assembly, and Application of
444 Patchy Particles, *Macromolecular Rapid Communications* 31 (2) (2010) 150–168.
445 doi:10.1002/marc.200900614.
- 446 [14] Z. Nie, W. Li, M. Seo, S. Xu, E. Kumacheva, Janus and ternary particles generated
447 by microfluidic synthesis: design, synthesis, and self-assembly, *J. Am. Chem. Soc.* 128
448 (2006) 9408–9412.

- 449 [15] T. Nisisako, Recent advances in microfluidic production of Janus droplets and parti-
450 cles, *Current Opinion in Colloid & Interface Science* 25 (Supplement C) (2016) 1–12.
451 doi:10.1016/j.cocis.2016.05.003.
- 452 [16] K. Nakahama, H. Kawaguchi, K. Fujimoto, A novel preparation of nonsymmetrical
453 microspheres using the langmuir-blodgett technique, *Langmuir* 16 (2000) 7882–7886.
- 454 [17] C. Kaewsaneha, P. Tangboriboonrat, D. Polpanich, M. Eissa, A. Elaissari, Preparation
455 of Janus colloidal particles via Pickering emulsion: An overview, *Colloids and Sur-
456 faces A: Physicochemical and Engineering Aspects* 439 (Supplement C) (2013) 35–42.
457 doi:10.1016/j.colsurfa.2013.01.004.
- 458 [18] L. Hong, S. Jiang, S. Granick, Simple Method to Produce Janus Colloidal Particles in
459 Large Quantity, *Langmuir* 22 (23) (2006) 9495–9499. doi:10.1021/la062716z.
- 460 [19] S. Jiang, M. Schultz, Q. Chen, J. Moore, S. Granick, Solvent-free syn-
461 thesis of Janus colloidal particles, *Langmuir* 24 (2008) 10073–10077.
462 doi:https://doi.org/10.1021/la800895g.
- 463 [20] S. Jiang, S. Granick, Controlling the geometry (Janus balance) of amphiphilic colloidal
464 particles, *Langmuir* 24 (2008) 2438–2445.
- 465 [21] A. Zenerino, C. Peyratout, A. Aimable, Synthesis of fluorinated ceramic Janus particles
466 via a Pickering emulsion method, *J. Colloid Interface Sci.* 450 (2015) 174–181.
- 467 [22] X. Xu, Y. Liu, Y. Gao, H. Li, Preparation of Au@silica Janus nanosheets
468 and their catalytic application, *Colloids Surf., A* 529 (2017) 613 – 620.
469 doi:https://doi.org/10.1016/j.colsurfa.2017.06.048.
- 470 [23] K. Panwar, M. Jassal, A. Agrawal, TiO₂-SiO₂ Janus particles with highly enhanced
471 photocatalytic activity, *RSC Adv.* 6 (2016) 92754–92764. doi:10.1039/C6RA12378C.
- 472 [24] E. Y. Hwang, J. S. Lee, D. W. Lim, Oppositely charged, stimuli-responsive
473 anisotropic nanoparticles for colloidal self-assembly, *Langmuir* 35 (13) (2019) 4589–4602.
474 doi:10.1021/acs.langmuir.8b04002.

- 475 [25] E. Y. Hwang, M. J. Kang, A. Basheer, D. W. Lim, Tunable decoupling of dual drug
476 release of oppositely charged, stimuli-responsive anisotropic nanoparticles, *ACS Applied*
477 *Materials & Interfaces* 12 (1) (2020) 135–150. doi:10.1021/acsami.9b15485.
- 478 [26] L. Hong, A. Cacciuto, E. Luitjen, S. Granick, Clusters of charged janus spheres, *Nano*
479 *Letters* 6 (2006) 2510–2514.
- 480 [27] A. Bianchi, G. Kahl, C. Likos, Inverse patchy colloids: from microscopic description to
481 mesoscopic coarse-graining, *Soft Matter* 7 (2011) 8313.
- 482 [28] A. Bianchi, P. van Oostrum, C. Likos, G. Kahl, Inverse patchy colloids: Synthesis,
483 modeling and self-organization, *Curr. Opin. Colloid Interface Sci.* 30 (2017) 8–15.
- 484 [29] M. Piechowiak, A. Videcoq, F. Rossignol, C. Pagnoux, C. Carrion, M. Cerbelaud,
485 R. Ferrando, Oppositely charged model ceramic colloids: Numerical predictions and
486 experimental observations by confocal laser scanning microscopy, *Langmuir* 26 (2010)
487 12540–12547, DOI: 10.1021/la101027d.
- 488 [30] K. Lebdioua, A. Aimable, M. Cerbelaud, A. Videcoq, C. Peyratout, Influence of different
489 surfactants on pickering emulsions stabilized by submicronic silica, *J. Colloid Interface*
490 *Sci.* 520 (2018) 127–133, DOI: 10.1016/j.jcis.2018.03.019.
- 491 [31] N. Kamarudin, A. Jalil, S. Triwahyono, N. Salleh, A. Karim, R. Mukti, B. Hameed,
492 A. Ahmad, Role of 3-aminopropyltriethoxysilane in the preparation of mesoporous silica
493 nanoparticles for ibuprofen delivery: Effect on physicochemical properties, *Microporous*
494 *and Mesoporous Materials* 180 (2013) 235 – 241.
- 495 [32] D. M. Schlipf, S. E. Rankin, B. L. Knutson, Selective external surface functionalization
496 of large-pore silica materials capable of protein loading, *Microporous and Mesoporous*
497 *Materials* 244 (2017) 199 – 207. doi:https://doi.org/10.1016/j.micromeso.2016.10.023.
- 498 [33] N. Nishiyama, K. Horie, T. Asakura, Adsorption behavior of a silane coupling agent
499 onto a colloidal silica surface studied by ²⁹si nmr spectroscopy, *Journal of Colloid and*
500 *Interface Science* 129 (1989) 113 – 119.

- 501 [34] F. Cuoq, A. Masion, J. Labille, J. Rose, F. Ziarelli, B. Prelot, J.-Y. Bottero, Preparation
502 of amino-functionalized silica in aqueous conditions, *Applied Surface Science* 266 (2013)
503 155–160.
- 504 [35] H. Schmidt, H. Scholze, A. Kaiser, Principles of hydrolysis and condensation reaction of
505 alkoxysilanes, *Journal of Non-crystalline Solids* 63 (1984) 1–11.
- 506 [36] M. Cerbelaud, K. Lebdioua, C. T. Tran, B. Crespín, A. Aimable, A. Videcoq, Brownian
507 dynamics simulations of one-patch inverse patchy particles, *Phys. Chem. Chem. Phys.*
508 21 (2019) 23447–23458. doi:10.1039/C9CP04247D.
- 509 [37] B. Derjaguin, L. Landau, Theory of the stability of strongly charged lyophobic sols and of
510 the adhesion of strongly charged particles in solution of electrolytes., *Acta Physicochim.*
511 URSS 14 (1941) 633–662, DOI: 10.1016/0079–6816(93)90013–L.
- 512 [38] E. Verwey, J. Overbeek, *Theory of the Stability of Lyophobic Colloids*, Elsevier, Am-
513 terdam, 1948.
- 514 [39] L. Bergström, Hamaker constants for inorganic materials, *Adv. Colloid Interface Sci.* 70
515 (1997) 125–169–A163.
- 516 [40] R. Hogg, T. Healy, D. Fuerstenau, *Trans. Fraday Soc.* 62 (1966) 1638–1651.
- 517 [41] C. T. Tran, B. Crespín, M. Cerbelaud, A. Videcoq, Brownian dynamics simulation on
518 the GPU: Virtual colloidal suspensions, in: F. Jaillet, F. Zara, G. Zachmann (Eds.),
519 *Workshop on Virtual Reality Interaction and Physical Simulation*, The Eurographics
520 Association, 2015. doi:10.2312/vrphys.20151332.
- 521 [42] W. Russel, D. Saville, W. Schowalter, *Colloidal Dispersions*, Cambridge University Press:
522 Cambridge, England, 1989.
- 523 [43] P.-Y. Hsiao, Chain morphology, swelling exponent, persistence length, like-charge attrac-
524 tion, and charge distribution around a chain in polyelectrolyte solutions: Effects of salt
525 concentration and ion size studied by molecular dynamics simulations, *Macromolecules*
526 39 (2006) 7125–7137.

- 527 [44] A. Das, P.-Y. Hsiao, Charged dendrimers in trivalent salt solutions under the action of
528 dc electric fields, *J. Phys. Chem.B* 118 (2014) 6265–6276.
- 529 [45] H. Rezvantlab, D. J. Beltran-Villegas, R. G. Larson, Rotator-to-lamellar phase transi-
530 tion in janus colloids driven by pressure anisotropy, *Phys. Rev. Lett.* 117 (2016) 128001.
531 doi:10.1103/PhysRevLett.117.128001.
- 532 [46] D. J. Beltran-Villegas, B. A. Schultz, N. H. P. Nguyen, S. C. Glotzer, R. G. Larson,
533 Phase behavior of janus colloids determined by sedimentation equilibrium, *Soft Matter*
534 10 (2014) 4593–4602. doi:10.1039/C3SM53136H.
- 535 [47] C.-P. Lafrance, A. Nabet, R. Prud’homme, M. Pézolet, On the relationship between the
536 order parameter and the shape of orientation distributions, *Can. J. Chem.* 73 (9) (1995)
537 1497–1505.
- 538 [48] R. J. Greasty, R. M. Richardson, S. Klein, D. Cherns, M. R. Thomas, C. Pizzey, N. Ter-
539 rill, C. Rochas, Electro-induced orientational ordering of anisotropic pigment nanopar-
540 ticles, *Philos. Trans. R. Soc., A* 371 (1988) (2013) 20120257.
- 541 [49] M. Sabapathy, R. Mathews, E. Mani, Self-assembly of inverse patchy colloids with tun-
542 able patch coverage, *Phys. Chem. Chem. Phys.* 19 (2017) 13122–13132.
- 543 [50] J. Dempster, M. O. de la Cruz, Aggregation of heterogeneously charged colloids, *ACS*
544 *Nano* 10 (2016) 5909–5915.
- 545 [51] M. Cerbelaud, A. Videcoq, P. Abélard, C. Pagnoux, F. Rossignol, R. Ferrando, Self-
546 assembly of oppositely charged particles in dilute ceramic suspensions: predictive role
547 of simulations, *Soft Matter* 6 (2009) 370–382.
- 548 [52] D. Bochicchio, A. Videcoq, A. Studart, R. Ferrando, Compact and ordered colloidal
549 clusters from assembly/disassembly cycles: A numerical study, *Journal of Colloid and*
550 *Interface Science* 440 (2015) 198 – 203.
- 551 [53] A. Stukowski, Visualization and analysis of atomistic simulation data with OVITO—the
552 Open Visualization Tool, *Modelling and simulations in materials science and Engineering*
553 18. doi:10.1088/0965-0393/18/1/015012.